RESEARCH ARTICLE

Functional Analysis of Rhomboid Proteases during *Toxoplasma* Invasion

Bang Shen, Jeffrey S. Buguliskis, Tobie D. Lee, L. David Sibley

Department of Molecular Microbiology, Washington University School of Medicine, St. Louis, Missouri, USA

ABSTRACT **Host cell invasion by *Toxoplasma gondii* and other apicomplexan parasites requires transmembrane adhesins that mediate binding to receptors on the substrate and host cell to facilitate motility and invasion. Rhomboid proteases (ROMs) are thought to cleave adhesins within their transmembrane segments, thus allowing the parasite to disengage from receptors and completely enter the host cell. To examine the specific roles of individual ROMs during invasion, we generated single, double, and triple knockouts for the three ROMs expressed in *T. gondii* tachyzoites. Analysis of these mutants demonstrated that ROM4 is the primary protease involved in adhesin processing and host cell invasion, whereas ROM1 or ROM5 plays negligible roles in these processes. Deletion of ROM4 blocked the shedding of adhesins such as MIC2 (microneme protein 2), causing them to accumulate on the surface of extracellular parasites. Increased surface adhesins led to nonproductive attachment, altered gliding motility, impaired moving junction formation, and reduced invasion efficiency. Despite the importance of ROM4 for efficient invasion, mutants lacking all three ROMs were viable and MIC2 was still efficiently removed from the surface of invaded mutant parasites, implying the existence of ROM-independent mechanisms for adhesin removal during invasion. Collectively, these results suggest that although ROM processing of adhesins is not absolutely essential, it is important for efficient host cell invasion by *T. gondii*.**

IMPORTANCE **Apicomplexan parasites such as *Toxoplasma gondii* express surface proteins that bind host cell receptors to aid invasion. Many of these adhesins are subject to cleavage by rhomboid proteases (ROMs) within their transmembrane segments during invasion. Previous studies have demonstrated the importance of adhesin cleavage for parasite invasion and proposed that the ROMs responsible for processing would be essential for parasite survival. In *T. gondii*, ROM5 was thought to be the critical ROM for adhesin shedding due to its robust protease activity *in vitro* and posterior localization on the parasite surface. Here, we knocked out all three ROMs in *T. gondii* tachyzoites and found that ROM4, but not ROM5, was key for adhesin cleavage. However, none of the ROMs individually or in combination was essential for cell entry, further emphasizing that essential pathways such as invasion typically rely on redundant pathways to ensure survival.**

Received 15 August 2014 **Accepted** 29 September 2014 **Published** 21 October 2014

Citation Shen B, Buguliskis JS, Lee TD, Sibley LD. 2014. Functional analysis of rhomboid proteases during *Toxoplasma* invasion. mBio 5(5):e01795-14. doi:10.1128/mBio.01795-14.

Editor Louis M. Weiss, Albert Einstein College of Medicine

Address correspondence to L. David Sibley, sibley@wusm.wustl.edu.

Toxoplasma gondii is an obligate intracellular pathogen infecting a wide range of animals as well as humans and can cause severe complications in immunocompromised individuals (1). Belonging to the phylum Apicomplexa, *T. gondii* shares with other members of this large group of parasites a common set of structures and mechanisms for host cell invasion (2). For the apicomplexan parasites that are of clinical and veterinary significance, such as *Plasmodium*, *Toxoplasma*, and *Cryptosporidium*, the invasion process provides a potential target for antiparasitic drug and vaccine design. However, this potential is largely unmet due to limited knowledge on the essential components of this process.

Host cell invasion by apicomplexan parasites is a multistep process that includes gliding motility, host cell attachment, and active penetration (2). Parasites contain specialized secretory organelles called micronemes and rhoptries that release proteins to mediate invasion (3). Micronemes discharge soluble and transmembrane proteins (referred to as MICs) to the parasite surface, where they form adhesive complexes (MIC2/M2AP [MIC2-associated protein], MIC3/MIC8, MIC1/MIC4/MIC6, etc.) that bind host receptors to mediate gliding motility and host cell attachment (4). After initial host cell binding, which is mediated by micronemal proteins, parasites secrete their rhoptry contents into host cells (5). Rhoptry proteins found in the neck of the organelle (referred to as RONs [*r*hoptry *n*eck proteins]) form the moving junction (MJ) (6, 7), a crucial structure for invasion that is formed by close opposition of host and parasite membranes and through which the parasite enters the host cell.

Micronemal adhesins undergo complex proteolytic processing after exocytosis (8). In *T. gondii*, three types of proteases, historically termed microneme protein protease 1 (MPP1), MPP2, and MPP3, are involved in processing adhesins (8). MPP2 trims the N terminus of MIC2 (9) and the C termini of M2AP and MIC4 (10). MPP3 cleaves M2AP and differs from MPP2 in terms of sensitivity to protease inhibitors (10). The specific proteases mediating

MPP2 and MPP3 activities have not yet been clearly identified, but recent work suggests that the micronemal subtilisin-like serine protease SUB1 is required for their activities (11). Parasites lacking SUB1 are impaired in host cell attachment, invasion, and gliding motility, suggesting that the processing of adhesins by MPP2 and MPP3 is important for these activities (11). MPP1 is responsible for the intramembrane cleavage of transmembrane adhesins such as MIC2, MIC6, and apical membrane antigen 1 (AMA1), resulting in the shedding of their extracellular domains to the supernatant (9, 12). MPP1 activity depends on rhomboid proteases (ROMs) (13, 14), which are membrane-spanning serine proteases that have the unique characteristic of cleaving substrates within their transmembrane domains (15–17).

Rhomboids recognize a cluster of helix-breaking residues near the external surface of the transmembrane domain of their substrates, typically rich in Ala and Gly (18, 19). Because they are not highly sequence specific, ROMs often work on substrates across widely different taxa, and COS cells have been widely used as a heterologous system to determine the protease activity and substrate specificity of ROMs (13, 20, 21). Rhomboids perform a variety of diverse functions in different taxa ranging from control of growth to signaling and adhesion, etc., and this depends on cleavage of a wide range of unrelated substrates (17). Hence, rhomboids recognize the conserved feature of a less stable helical region in the transmembrane domains of otherwise dissimilar substrates. ROMs also show unusual kinetics that do not depend on substrate affinity but rather are driven by access of the substrate to the catalytic site (22). Collectively, these features suggest that ROMs have been coopted from an earlier quality control system for detecting unfolded membrane proteins (22).

The genomes of apicomplexan parasites encode multiple ROMs: for example, *T. gondii* has six and *Plasmodium falciparun* has eight *ROM* genes (23, 24). Of the six *Toxoplasma* ROMs, ROM6 is predicted to be a mitochondrial PARL-like ROM (14). The other five display stage-specific expression, with *ROM1*, *ROM4*, and *ROM5* being expressed in tachyzoites; *ROM4* in bradyzoites; and *ROM1*, *ROM2*, and *ROM3* in sporozoites (13, 14). Given that many adhesins important for tachyzoite invasion, such as MIC2 and AMA1, are substrates for ROMs (13), it is of great interest to know the exact roles of the different ROMs expressed at the tachyzoite stage. Previous work has addressed the role of individual ROMs in *T. gondii* but has not established which, if any, of these proteases are essential. For example, *T. gondii* ROM1 (TgROM1) localizes to micronemes, and knockdown of *TgROM1* resulted in a mild growth defect (25). TgROM4 is evenly distributed on the plasma membrane (13), and conditional suppression of this gene caused reduced adhesin shedding and decreased invasion (26). Additionally, overexpression of a dominant negative mutant of *TgROM4* inhibited AMA1 cleavage and blocked parasite replication after invasion, suggesting signaling roles for AMA1 and TgROM4 (27). However, later studies did not find support for such roles, since a noncleavable mutant (28) and a complete knockout mutant (29) of AMA1 had normal intracellular replication, although they invaded less efficiently. TgROM5 also localizes to the surface but accumulates at the posterior end of the parasite membrane (13). In a heterologous system, TgROM5 displayed the highest activity against a broad range of substrates among all the *T. gondii* ROMs tested (13). Based on the posterior localization and robust protease activity, it was hypothesized that TgROM5 is the key ROM that cleaves surface adhesins during invasion to disengage adhesive interactions between the parasite and host cell receptors so that the parasite can fully enter the host cell (13).

In this study, we focused on the biological roles of the three ROMs (ROM1, ROM4, and ROM5) expressed in *T. gondii* tachyzoites. We generated gene knockouts and found that TgROM4 is the major tachyzoite ROM involved in surface adhesin processing and host cell invasion. Nonetheless, none of the ROMs were absolutely required for host cell penetration; however, intramembrane cleavage of micronemal adhesins was important for apical attachment and efficient host cell invasion by *T. gondii*.

RESULTS

Generation of *ROM* knockouts. Given its posterior localization and robust protease activity in a heterologous system, TgROM5 was proposed to be the key ROM shedding surface adhesins during invasion (13). Consistent with this, numerous attempts to knock out this gene by homologous replacement in the RH strain or its Δ*ku80* derivative were not successful (data not shown). In order to obtain genetically modified strains to study the biological functions of TgROM5, we used the previously described loxP-Cre technology to first flox the *TgROM5* locus and subsequently delete this gene by expressing Cre recombinase (30, 31). The general design of this strategy is outlined in Fig. 1A. To flox the endogenous locus, a construct that contains the coding sequence of the corresponding *ROM* gene and the selection marker HXGPRT (hypoxanthine-xanthine-guanine phosphoribosyltransferase) cassette flanked by two loxP sites, as well as homologous arms for recombination, was transfected into the RH Δ*ku80* Δ*hxgprt* strain. After mycophenolic acid and xanthine selection, homologous replacement clones containing the floxed locus were identified by diagnostic PCR (Fig. 1A). To delete the floxed *ROM* gene, a plasmid (pmin-Cre-eGFP) (31) expressing the Cre recombinase was transiently transfected and selected with 6-thioxanthine (for *HXGPRT* deletion). Positive knockout clones were identified by diagnostic PCR and Western blotting (Fig. 1).

Using this system, we were able to efficiently generate clean *TgROM5* knockouts (Δ*rom5*) (Fig. 1C and D). The nonessential nature of *TgROM5* made us suspect that it might have redundant functions with the other two tachyzoite *ROM* genes (i.e., *TgROM1* and *TgROM4*). To check this possibility, and to determine the specific roles of each *ROM*, we used the loxP-Cre strategy and generated Δ*rom1*, Δ*rom4*, and Δ*rom5* single knockouts as well as double (Δ*rom1* Δ*rom4*, Δ*rom1* Δ*rom5*, and Δ*rom4* Δ*rom5*) and triple (Δ*rom1* Δ*rom4* Δ*rom5*) knockouts (Fig. 1B to H), which were confirmed by diagnostic PCR and Western blotting (for *ROM4* and *ROM5*) (Fig. 1C to G). Δ*rom1* mutants were confirmed by additional PCRs to check the endogenous *ROM1* gene (Fig. 1H) due to the lack of anti-TgROM1 antibody for Western blot analysis.

The fact that all the *ROM* mutants, including the triple knockout, were able to grow in tissue culture suggests that these enzymes are not essential for parasite survival *in vitro*. There are two other nonmitochondrial *ROM* genes (i.e., *TgROM2* and *TgROM3*) that are not normally expressed at the tachyzoite stage (13), yet it remained possible that their expression was upregulated to compensate for the loss of ROM activity in our mutants. However, by quantitative real-time PCR (qRT-PCR), we detected very low levels of *TgROM2* and *TgROM3* transcripts in tachyzoites of the wild type (WT) and the triple knockout parasites, and there was no

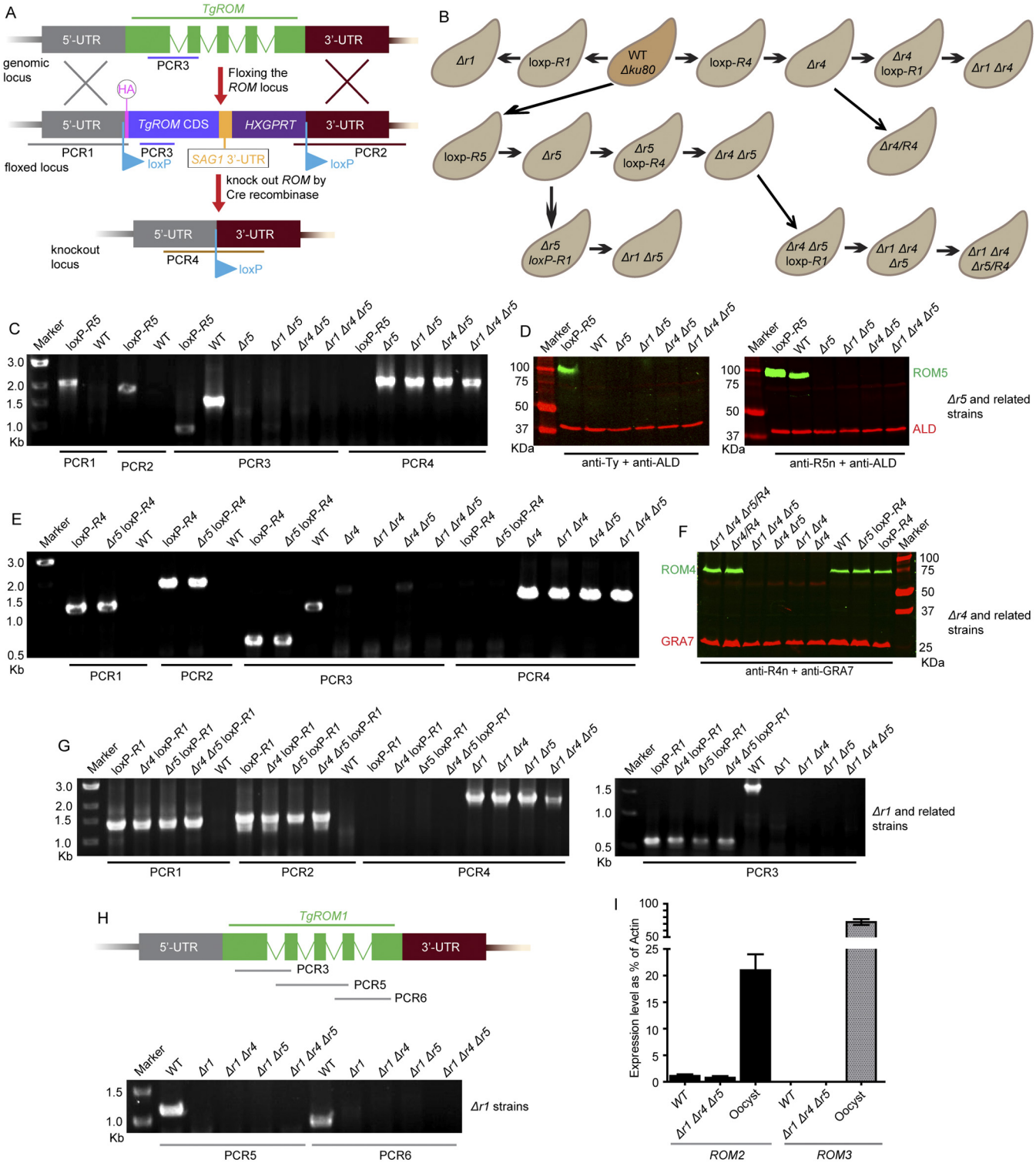

FIG 1 Generation of *ROM* knockouts using the loxP-Cre technology. (A) Schematic illustration of the strategy used to generate the knockouts. First, a construct containing a *ROM* coding sequence and the HXGPRT selection marker flanked by two loxP sites was transfected into an RH Δ*ku80* strain to generate a floxed *ROM* strain. Subsequently, a Cre-expressing plasmid was transiently introduced into the floxed *ROM* strains to generate *ROM* knockouts by Cre-mediated recombination at the loxP sites. All the floxed *ROM* genes were hemagglutinin tagged at the N terminus, and ROM5 had an additional Ty tag at the C terminus. Diagnostic PCRs used to identify the correct clones are indicated based on the following amplicons. PCR1 and PCR2 checked for the proper (5′ and 3′, respectively) integration of the floxing construct into the corresponding *ROM* locus. PCR3 checked the replacement of endogenous *ROM* locus by the corresponding floxed *ROM*. Due to the removal of introns, the floxed locus gave a smaller PCR3 product than did the endogenous locus. PCR4 checked the junction of loxP after *ROM* deletion. (B) Diagram of the strains constructed in this study and the order of their construction. (C) Diagnostic PCRs on *ROM5* deletion (Δ*r5*) and related strains. (D) Western blot analysis of Δ*r5* and related strains using mouse anti-Ty or mouse anti-R5n (against the N terminus of

(Continued)

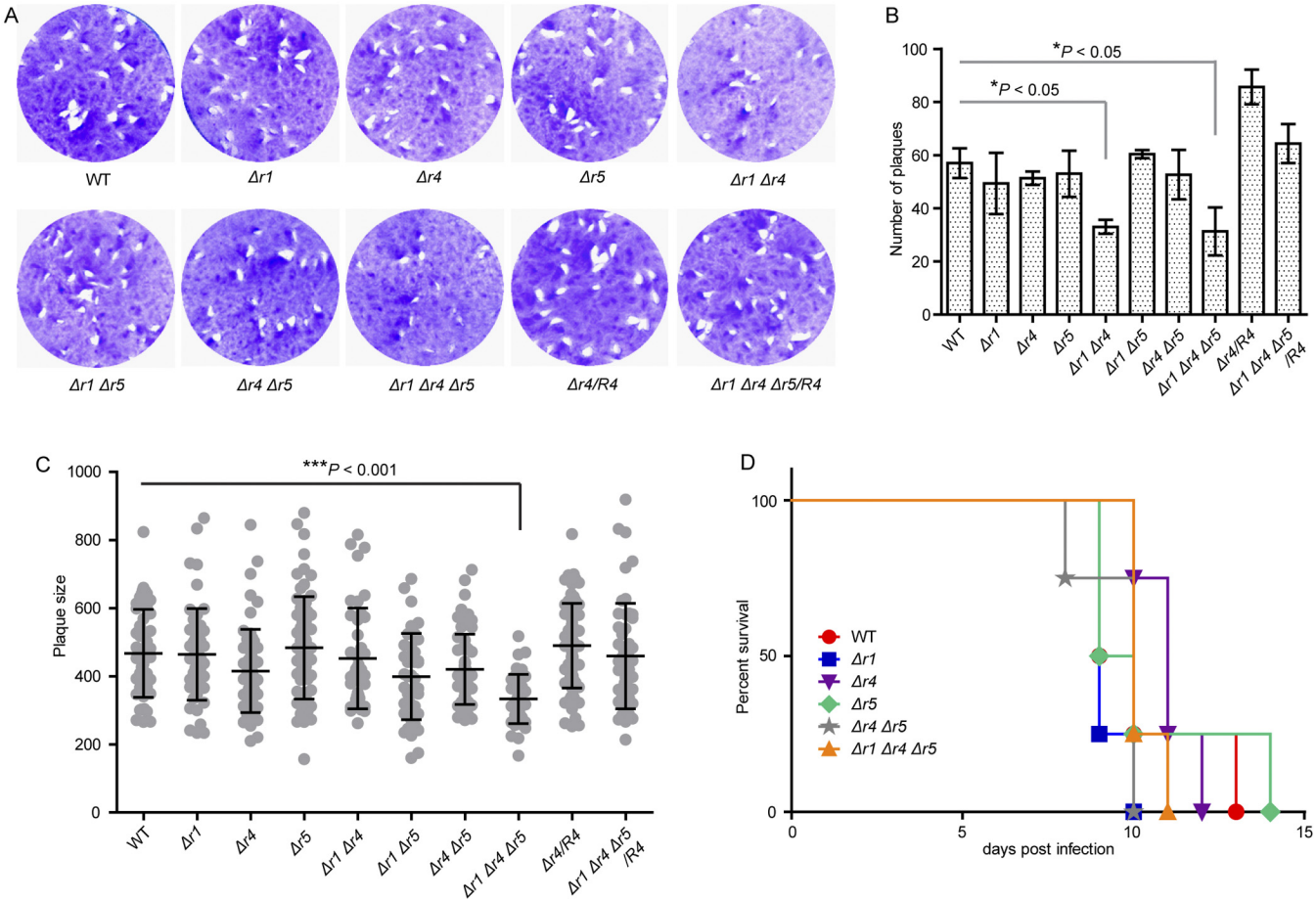

FIG 2 Growth of WT and *ROM* knockout parasites *in vitro* and *in vivo*. (A) Plaque assay examining growth of parasites in HFF cells. Plaques are visible as clear zones on the background of crystal violet-stained HFF monolayers. (B) Number of plaques observed from panel A. *, $P < 0.05$, one-way ANOVA with Bonferroni posttests of mutants versus WT. (C) Sizes of plaques in panel A. ***, $P < 0.001$, one-way ANOVA with Bonferroni posttests of mutants versus WT. Experiments (A to C) were repeated three times (each with triplicates) independently, and a representative one is shown here. (D) Virulence of *ROM* knockouts in CD-1 mice. Purified tachyzoites from indicated strains were intraperitoneally injected (200 parasites/mouse and 5 mice/parasite strain) into CD-1 mice, and the survival of mice was monitored.

significant difference between the two strains (Fig. 1I). These results indicate that *TgROM2* and *TgROM3* were not upregulated to compensate for the loss of ROM activities in the triple knockout. Collectively, these findings indicate that the three *ROM* genes expressed at the tachyzoite stage are not essential for parasite survival.

Growth of *ROM* knockouts *in vitro* and *in vivo*. To assess whether TgROM1, TgROM4, or TgROM5 played any role during parasite growth, we checked the ability of *ROM* knockout strains to form plaques on human foreskin fibroblast (HFF) monolayers. All of the *ROM* knockouts were able to produce plaques (Fig. 2A, B, and C), suggesting that none of the three *ROM* genes is essential for growth. Among repeated experiments, the Δ*rom1* Δ*rom4* Δ*rom5* triple knockout always produced fewer (40 to 60%) and smaller plaques (Fig. 2B and C) than did the WT strain. The Δ*rom1* Δ*rom4* double knockout also produced fewer (≈50%) plaques (Fig. 2B). Initially, we complemented Δ*rom4* and Δ*rom1* Δ*rom4* Δ*rom5* strains with *TgROM4* at the *UPRT* (uracil phosphoribosyltransferase) locus, which is a nonessential gene. Although growth and invasion defects were rescued, the expression of ROM4 was lower than that in the wild type (data not shown). Therefore, we complemented Δ*rom4* and Δ*rom1* Δ*rom4* Δ*rom5* strains with *TgROM4* at the endogenous locus to produce Δ*rom4*/*ROM4* and Δ*rom1* Δ*rom4* Δ*rom5*/*ROM4* strains, respectively (Fig. 1F; see also Fig. S1 in the supplemental material). Plaque

Figure Legend Continued

TgROM5). TgALD was detected by rabbit anti-ALD as a loading control. Li-Cor goat anti-mouse and -rabbit secondary antibodies were used to detect primary antibodies, and blots were scanned on the Li-Cor imaging system. (E) Diagnostic PCRs on *ROM4* deletion (Δ*r4*) and related strains. (F) Western blot analysis of Δ*r4* and related strains using rabbit anti-R4n (against the N terminus of TgROM4). TgGRA7 was detected by mouse anti-GRA7 as a loading control. Blots were developed and scanned as described above. (G) Diagnostic PCRs on all *ROM1* deletion (Δ*r1*) and related strains. (H) Additional PCRs confirming the loss of *ROM1* sequence in Δ*r1* strains. (I) Analysis of *TgROM2* and *TgROM3* expression levels in wild-type (WT) and triple knockout Δ*r1* Δ*r4* Δ*r5* parasites by qRT-PCR. RNA isolated from unsporulated oocysts was used as a positive control, and the messenger levels of *TgROM2* and *TgROM3* were expressed as a percentage of actin in each sample. Means ± standard deviations of results from three independent experiments ($n = 3$).

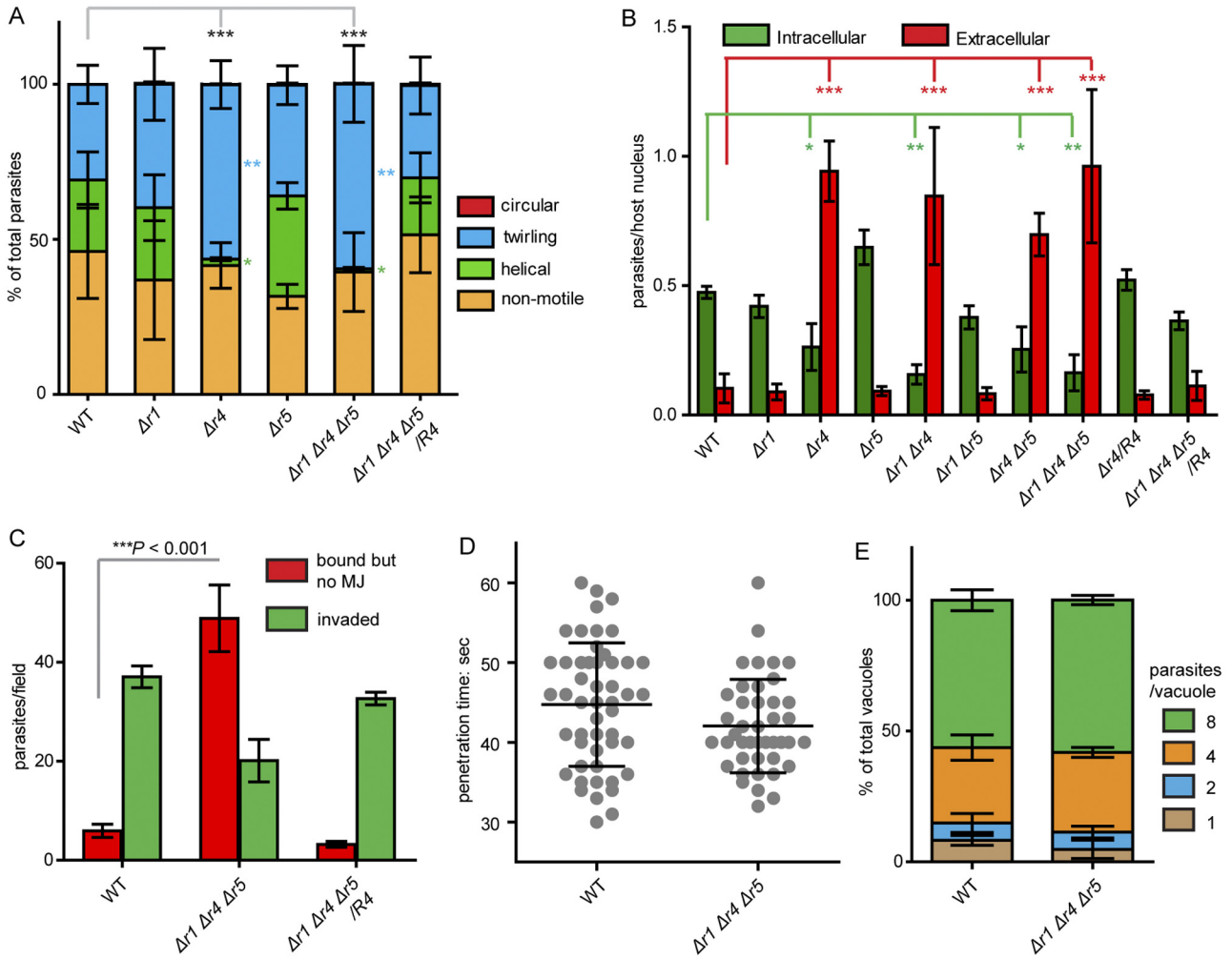

FIG 3 Gliding motility, host cell invasion, and intracellular replication of WT and *ROM* mutant parasites. (A) Motility of freshly egressed tachyzoites on BSA-coated coverslips determined by time-lapse microscopy. Purified parasites were added to prewarmed Ringer's buffer and imaged from 3 min at 1 frame/s. Means ± standard deviations from three independent experiments ($n = 3$). *, $P < 0.05$; **, $P < 0.01$; ***, $P < 0.001$. Two-way ANOVA was used to determine the overall difference (black asterisks) between each mutant and WT, and subsequent Bonferroni posttests (blue and green asterisks) were used to compare each motility type of the selected mutant to that of the WT. (B) Host cell invasion efficiencies determined by a two-color staining protocol that distinguishes intracellular from extracellular parasites. Representative data (means ± standard deviations) from three independent experiments (each with triplicates) with similar outcomes. *, $P \leq 0.05$; **, $P \leq 0.01$; ***, $P \leq 0.001$. Two-way ANOVA with Bonferroni posttests of mutants versus WT. (C) Moving junction formation during invasion determined by immunostaining. Naturally egressed parasites were used to challenge an HFF monolayer for 5 min at 37°C, and cells were immediately fixed for staining (see Fig. S2 in the supplemental material for details). Parasites falling into the indicated categories were counted and graphed as means ± standard deviations. Representative data (means ± standard deviations) from three independent experiments (each with triplicates) with similar outcomes. ***, $P \leq 0.001$, two-way ANOVA with Bonferroni posttests. (D) Speed of invasion as determined by time-lapse video microscopy. Freshly purified parasites were used to invade HFF monolayers at 37°C and imaged for 3 min at 1 frame/s. The time spent during active penetration of each invaded parasite (from apical binding to complete internalization) was determined. Each dot represents one invasion event. Means ± standard deviations of results from two independent experiments (each with >3 replicates). (E) Intracellular replication of WT and the triple knockout parasites, which was determined by counting the number of parasites in each parasitophorous vacuole 18 h after invasion. Parasites were visualized by MAb DG52 staining of SAG1 followed by Alexa 488-conjugated goat anti-mouse secondary antibody. Means ± standard deviations ($n = 6$) of results from two independent experiments (each with triplicates).

assays using these complemented lines indicated that *TgROM4* was able to fully complement the growth defect of the triple knockout (Fig. 2A, B, and C). In an animal infection experiment, the survival of mice infected with *ROM* mutants was very similar to that of mice infected with WT parasites (Fig. 2D), indicating that these ROMs are not essential for parasite growth *in vivo*. Taken together, these results suggest that while ROMs are important for optimal growth of tachyzoites in tissue culture, they are not absolutely essential for survival or virulence.

TgROM4 is important for efficient parasite motility and host cell invasion. To test the roles of ROMs in parasite motility, we used video microscopy to compare the motility patterns of WT and mutant parasites. When freshly egressed parasites were allowed to glide on a bovine serum albumin (BSA)-coated glass surface, Δ*rom4* mutants displayed significantly reduced helical gliding but increased twirling (Fig. 3A). This alteration was fully restored by *TgROM4* complementation (Fig. 3A). Δ*rom1* or Δ*rom5* mutations (if not combined with Δ*rom4*) did not cause any

obvious motility change (Fig. 3A), suggesting that TgROM4 is the primary tachyzoite ROM important for efficient gliding motility.

To test the role of ROMs in host cell invasion, we performed a two-color invasion assay that distinguishes extracellular parasites from intracellular parasites. Consistent with a previous report (26), TgROM4 was important for efficient invasion, as any mutant harboring Δ*rom4* displayed impaired invasion (Fig. 3B). In addition to reduced invasion, we also observed significantly more bound but noninvaded parasites with all Δ*rom4* strains (Fig. 3B), suggesting that increased nonproductive host cell attachment occurs in these mutants. Complementing with *TgROM4* restored the invasion efficiency and reduced the attachment to normal levels (Fig. 3B), confirming that *TgROM4* is responsible for these phenotypes. Deletion of *TgROM1* or *TgROM5*, unless in combination with Δ*rom4*, did not have any obvious effects on invasion efficiency or parasite attachment (Fig. 3B). The invasion phenotypes of the *ROM* deletion mutants matched well with their motility phenotypes. Taken together, these results suggest that TgROM4 plays a dominant role in parasite motility and host cell invasion, relative to other ROMs.

Initiation but not active penetration of invasion is impaired in Δ*rom4* parasites. Having demonstrated that Δ*rom4* mutants have reduced efficiency in host cell invasion, we wanted to further identify at what step of invasion they are impaired. First, we checked their ability to establish a MJ, a key step during invasion that initiates active penetration (32). Following a pulse invasion (5 min), the MJ was identified by the ring-like staining pattern of TgRON4 (see Fig. S2 in the supplemental material). With the WT strain, most parasites invaded successfully and did not display TgRON4 rings (classified as "invaded," Fig. 3C), but instead they had a TgRON4 dot at the posterior end (see Fig. S2). A small portion of parasites were attached but did not show any TgRON4 staining (classified as "bound but no MJ," Fig. 3C; see also Fig. S2), suggesting that they had not initiated invasion yet. Due to the high speed of invasion (see below), only a few parasites were observed in the process of invasion and they showed ring-shaped staining of TgRON4 (classified as "invading," Fig. S2). In contrast, with the triple Δ*rom1* Δ*rom4* Δ*rom5* knockout, we observed fewer invaded parasites and significantly more parasites that were attached but failed to form an MJ (Fig. 3C). This pattern suggests that Δ*rom4* mutants engage in nonproductive attachment that does not lead to MJ formation, thus impeding invasion. These phenotypes were fully restored by *TgROM4* complementation (Fig. 3C), indicating that they were caused by loss of *ROM4*.

Next, we looked at the speed of invasion, as determined by time-lapse video microscopy and expressed as the time required to penetrate a host cell (from apical binding to complete internalization). We compared the invasion speed of the Δ*rom1* Δ*rom4* Δ*rom5* triple knockout to that of WT parasites. Although triple knockout parasites invaded less frequently, those parasites that did invade penetrated the host cells at the same speed as did WT parasites (Fig. 3D). This finding suggests that ROMs likely do not play a role in the active penetration process.

Previous work using a dominant negative mutant of *TgROM4* suggested that TgROM4 played a critical role in parasite replication by cleaving TgAMA1 to initiate replication after invasion (27). We reexamined this requirement using our *ROM* mutants but found that even the Δ*rom1* Δ*rom4* Δ*rom5* parasites replicated normally once they successfully invaded (Fig. 3E), indicating that these ROMs are not required for intracellular replication.

Cleavage of micronemal adhesins in *ROM* mutants. Next, we sought to determine the contribution of ROMs in processing micronemal adhesins such as MIC2 and AMA1, which are known substrates for ROMs (13, 28) and important for host cell infection (33, 34). We examined the release of the ectodomains of MIC2 and AMA1 into culture supernatant upon stimulation of microneme secretion. All mutants lacking *ROM4* were completely defective in MIC2 processing (Fig. 4A), whereas Δ*rom1* or Δ*rom5* mutants (unless in combination with Δ*rom4*) did not show any defects (Fig. 4A). The cleavage pattern of AMA1 in *ROM* mutants was very similar to that of MIC2, although overall shedding of AMA1 was much less efficient as seen by comparing the ratio of proteins in the supernatant to those in pellet (Fig. 4A). Similarly to MIC2, only Δ*rom4* mutants had dramatic reduction of AMA1 cleavage (Fig. 4A). For control purposes, we looked at the discharge of the nontransmembrane micronemal protein MIC5 (35), which is not a substrate for rhomboids. All the strains tested here secreted MIC5 at similar levels (Fig. 4A). Taken together, these findings indicate that none of the *ROM* mutants had defects in microneme secretion (i.e., release of adhesins from micronemes to the parasite surface) and that the reduced shedding of MIC2 and AMA1 into supernatant observed in Δ*rom4* mutants was due to the inhibition of intramembrane cleavage. These results also suggest that TgROM4 is the major tachyzoite ROM responsible for shedding of MIC adhesins, whereas the other two play minor roles in this process.

MIC2 was enriched on the parasite surface of Δ*rom4* mutants. To further check the inability of Δ*rom4* mutants to process MIC adhesins, we induced microneme secretion and subsequently quantified surface MIC2 levels by immunostaining and flow cytometry analysis. As expected, all mutants containing Δ*rom4* accumulated significantly more MIC2 on the surface than did WT parasites (Fig. 4B). In contrast, Δ*rom1* and Δ*rom5* (if not combined with Δ*rom4*) mutants had surface MIC2 levels similar to that of WT parasites (Fig. 4B). In addition, surface MIC2 was almost completely shed in WT and other *TgROM4*-expressing parasites, since the signals for their surface MIC2 staining were very close to that of the negative control (Neg IgG, Fig. 4B). As a control, SAG1 staining was indistinguishable in all strains (WT and mutants) and was significantly higher than the control IgG staining (Fig. 4C).

We also visualized surface MIC2 by fluorescence microscopy after induction of microneme secretion. Consistent with the flow cytometry analysis, the levels of surface MIC2 on extracellular WT, Δ*rom1*, and Δ*rom5* parasites were close to background, whereas those in Δ*rom4*-containing mutants were greatly elevated (Fig. 4D). Together, these results indicate that ROM4 is needed to efficiently cleave MIC2 from the parasite surface.

Removal of micronemal adhesins from parasite surface during active invasion. Next, we sought to determine the fate of surface adhesins during active host cell invasion as monitored by quantitative immunofluorescence microscopy. Following induction of microneme secretion to release adhesins to the surface, parasites were allowed to invade host cells for 5 min and surface adhesin levels were measured by fluorescence microscopy. In both WT and Δ*rom1* Δ*rom4* Δ*rom5* parasites, AMA1 was evident on the surface of both extracellular and fully invaded parasites (Fig. 5A), consistent with the observation that it is not efficiently shed by extracellular parasites (Fig. 4A). In quantifying the fluorescent signals of invaded versus noninvaded parasites, we observed that

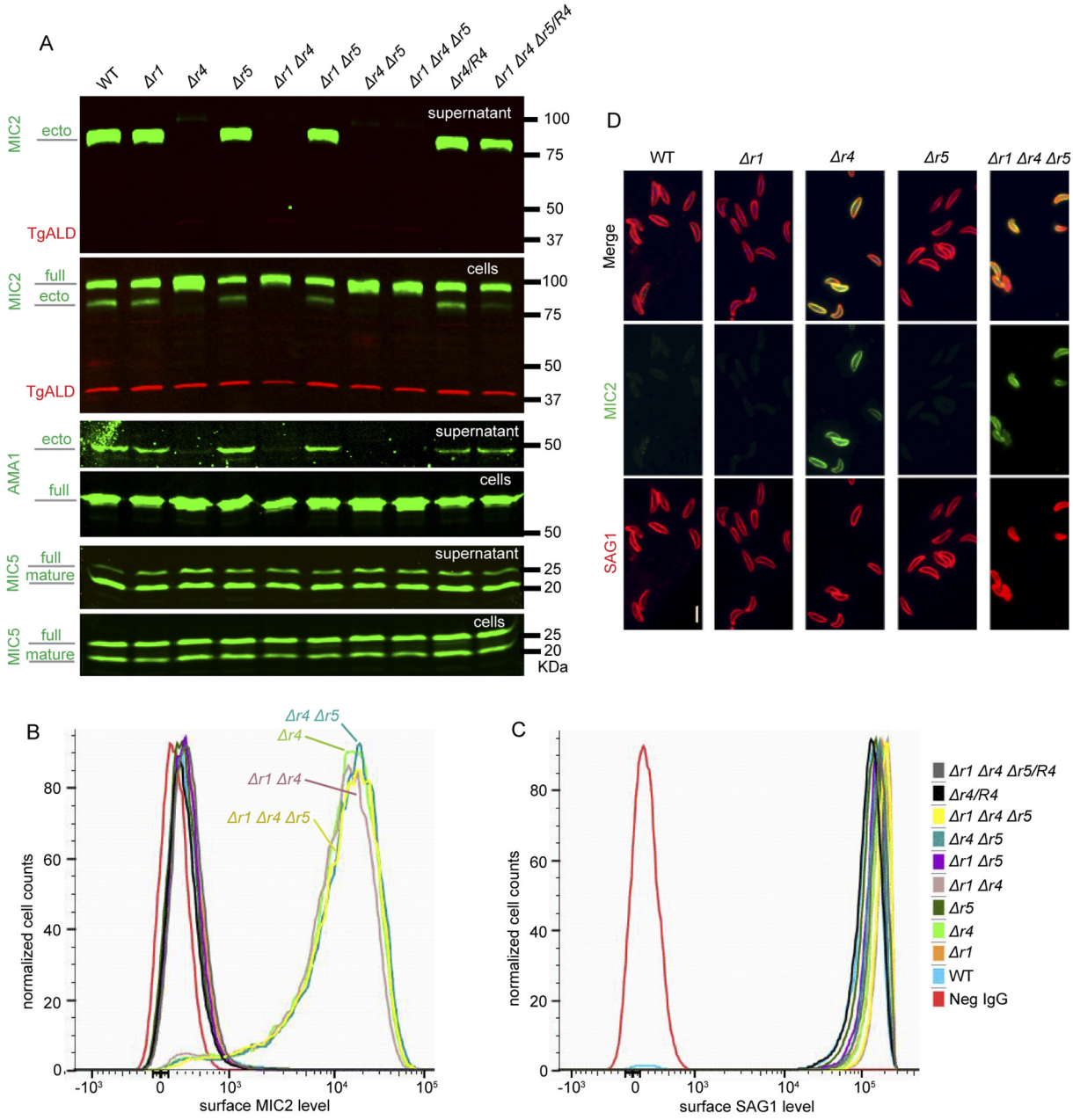

FIG 4 Cleavage and surface accumulation of micronemal adhesins in *ROM* mutants. (A) Microneme secretion assay assessing the cleavage of transmembrane adhesins in *ROM* mutants. Microneme secretion was induced with 3% FBS and 1% ethanol, and the supernatants were separated from pelleted cells and subject to Western blot analysis. MIC2 and AMA1 were detected by monoclonal antibodies 6D10 and B3.90, respectively. TgALD was detected by rabbit anti-TgALD as a loading for pellet fractions and a cell lysis control for supernatant fractions. The nontransmembrane micronemal protein MIC5 detected with rabbit anti-TgMIC5 served as a microneme secretion control. Primary antibodies were visualized by Li-Cor secondary antibodies, and blots were developed on the Li-Cor imaging system. ecto, ectodomain; full, full length. (B and C) Accumulation of adhesins on parasite surface as determined by flow cytometry analysis. Following the induction of microneme secretion as in panel A, parasites were fixed and surface adhesins were stained with corresponding antibodies (6D10 for MIC2 in panel B and DG52 for SAG1 in panel C) and quantified by flow cytometry after Alexa 488-conjugated goat anti-mouse secondary antibody staining. WT parasites stained with mouse IgG (Neg IgG) were used as a negative control to set the gates. (D) Fluorescence microscopy examining surface protein levels. Samples were processed in the same way as in panel B but costained with 6D10 (followed by Alexa 488-conjugated secondary antibody, green channel) and rabbit anti-SAG1 (followed by Alexa 594-conjugated secondary antibody, red channel) for microscopic examination. Bar, 5 μm.

AMA1 levels on extracellular parasites were slightly higher than that of intracellular parasites in both strains (Fig. 5B). This is likely due to the difference of antibody accessibility, since similar differences were also observed for SAG1 levels (Fig. 5B). In contrast to AMA1, MIC2 was detected on extracellular triple mutant parasites but was undetectable on the surface of invaded parasites in both WT and the triple knockout strain (Fig. 5A). This was expected for WT cells, since the above-mentioned studies clearly demonstrated that MIC2 was almost completely cleaved from the surface by TgROM4 (Fig. 4B and D). However, extracellular Δ*rom1* Δ*rom4*

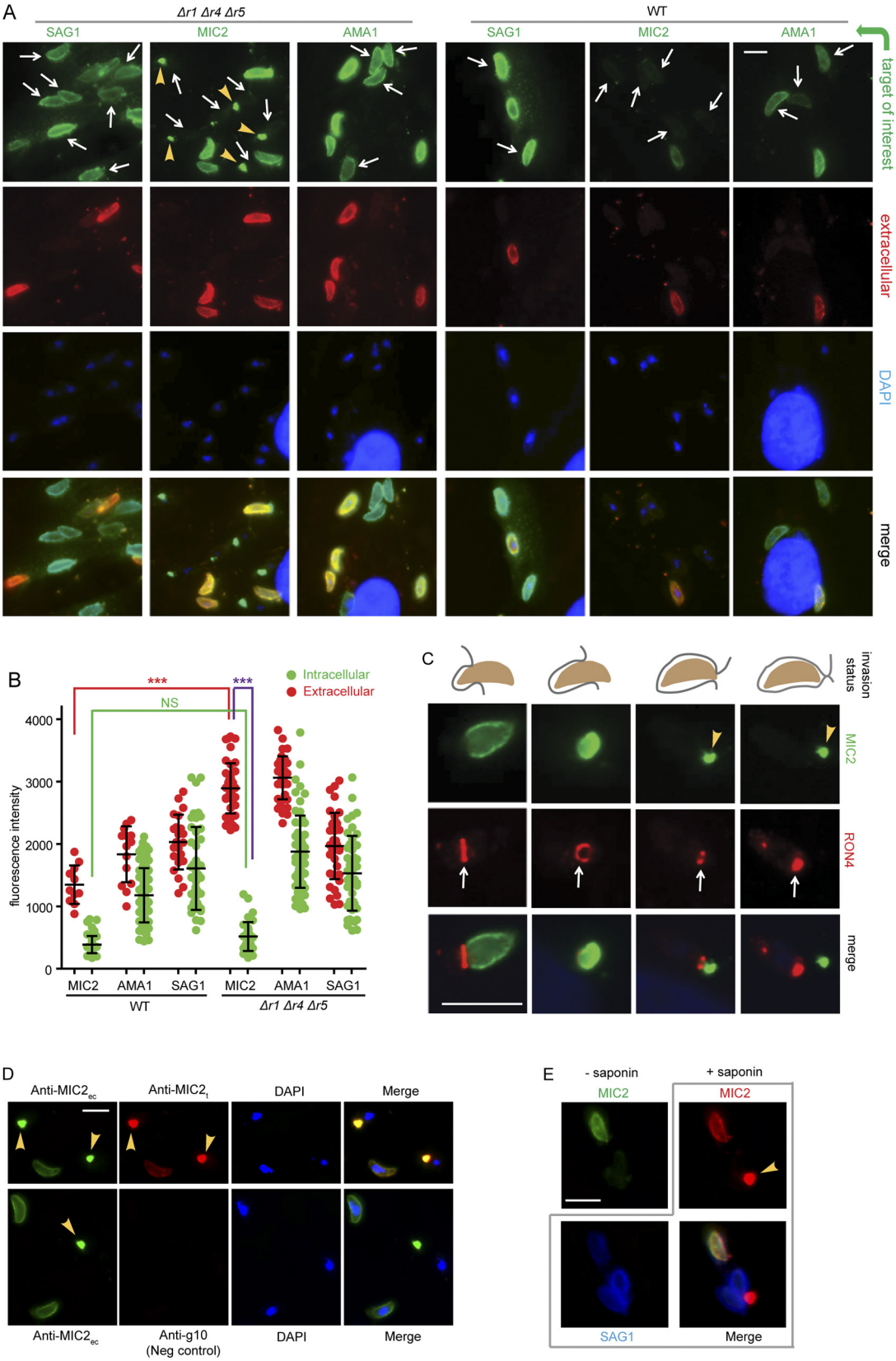

FIG 5 Fate of surface MIC2 during host cell invasion in WT and Δ*rom1* Δ*rom4* Δ*rom5* parasites. (A) Immunofluorescence staining of parasite surface antigens after host cell invasion. Parasites preinduced for microneme secretion were allowed to infect HFF monolayers for 5 min. Cells were then fixed, and extracellular parasites were stained with rabbit anti-SAG1. Following saponin permeabilization, parasites were stained with antibodies to AMA1 (MAb B3.90), MIC2 (MAb

(Continued)

Δ*rom5* parasites accumulated MIC2 on the surface (Fig. 4B and D); therefore, the lack of detectable MIC2 on invaded mutant parasites was surprising. Quantification of fluorescent signals clearly showed that extracellular Δ*rom1* Δ*rom4* Δ*rom5* parasites exhibited much higher surface MIC2 levels than did extracellular WT parasites (Fig. 5B). However, once invaded, the two strains displayed similar (undetectable) levels of MIC2 on the surface (Fig. 5B), indicating that there is a ROM-independent mechanism to remove MIC2 from surface during invasion.

To more carefully track the removal of MIC2 relative to invading parasites in the triple knockout, we localized MIC2 and the MJ protein RON4 after a short invasion pulse (2 min). Interestingly, as soon as invasion started, the invaded portion of the parasite lacked any detectable MIC2, whereas the part behind the MJ (defined by the TgRON4 ring) was strongly stained (Fig. 5C). For parasites that were mostly inside the host cell, MIC2 staining was localized to a dot right behind the TgRON4 ring (Fig. 5C). After the parasite was fully internalized, the MIC2 dot was further separated from the TgRON4-containing structure (Fig. 5C). These results demonstrated that as soon as a parasite has passed through the MJ, the accumulated surface MIC2 is removed, by a yet-unknown mechanism.

The dot structure of MIC2 was frequently found to be in the vicinity of invaded Δ*rom1* Δ*rom4* Δ*rom5* parasites (yellow arrowheads, Fig. 5A), consistent with the accumulation of MIC2 at the site of host entry. To check the integrity of MIC2 molecules in these dots, we stained them with two antibodies, one for the ectodomain of MIC2 ($MIC2_{ec}$) and the other for the cytoplasmic tail ($MIC2_t$). Costaining with these two antibodies indicated that MIC2 dots contained full-length MIC2 protein since they were positively stained by both antibodies (Fig. 5D). In addition, we looked at the location of MIC2 dots relative to host cells by checking whether they were on the host cell surface or inside host cells. For this purpose, we stained them before and after saponin permeabilization with differently labeled $MIC2_{ec}$ antibodies. Interestingly, surface MIC2 on noninvaded parasites was easily detected before saponin treatment. However, MIC2 dots were detectable only after permeabilization (Fig. 5E), indicating that they were inside the host cell membrane.

DISCUSSION

Rhomboids are known to process apicomplexan transmembrane adhesins that are required for host cell recognition, suggesting that these proteases would also be important for host cell invasion (12, 13, 20, 36). However, because parasites express multiple ROMs with potentially overlapping substrate specificities (23, 24), the exact biological functions of individual proteases have been difficult to define. In the present study, we took a genetic approach to study the functions of ROM proteases in *T. gondii*. We generated single, double, and triple knockout mutants for the three *ROM* genes (*ROM1*, *ROM4*, and *ROM5*) expressed in *T. gondii* tachyzoites to assess their functions. Analysis of these mutants indicates that only *ROM4* is required for efficient adhesin processing and host cell invasion, while *ROM1* and *ROM5* play negligible roles. Δ*rom4* mutants were unable to cleave adhesins like MIC2, which accumulated on the surface of extracellular parasites and led to impaired gliding motility, unproductive host cell attachment, and reduced invasion efficiency. However, mutants lacking individual or all three ROMs (i.e., the Δ*rom1* Δ*rom4* Δ*rom5* mutant) were viable, indicating that intramembrane cleavage of adhesins by ROM proteases is not essential. In addition, MIC2 that was secreted to the surface of Δ*rom4* mutants was still efficiently removed by a ROM-independent mechanism during active host cell entry. Taken together, these results demonstrate that, although not absolutely essential, ROM4 is the major tachyzoite ROM involved in cleaving micronemal adhesins on the parasite surface, where it serves to promote efficient apical attachment and facilitate invasion.

Proteolytic shedding of transmembrane micronemal adhesins from the membrane is a common feature of AMA1, MIC2, MIC6, MIC8, and MIC12 in *T. gondii* (8, 9, 37). Shedding is important for adhesin function, as shown by several previous studies. Mutations upstream of the transmembrane domain that block MIC2 shedding have a dominant negative effect, leading to increased host cell adhesion but reduced invasion (38). Similarly, mutations in the transmembrane domain that disrupt AMA1 shedding also decrease invasion efficiency (28). Shedding of these adhesins is mediated by intramembrane cleavage (10, 12, 28), suggesting the involvement of ROMs. Indeed, when assayed in a heterologous system, TgROM5 displayed robust ROM activity against a variety of substrates that included MIC2 and AMA1 (13, 28). However, the exact protease(s) that is responsible for adhesin shedding *in vivo* and its biological substrate specificity are not known, partially due to the overlapping expression of multiple ROMs in *T. gondii* tachyzoites.

In the present study, we knocked out the three *ROM* genes (*ROM1*, *ROM4*, and *ROM5*) expressed in tachyzoites, individu-

Figure Legend Continued

6D10), or SAG1 (MAb DG52). Primary antibodies were visualized by Alexa 594-conjugated goat anti-rabbit (red channel) and Alexa 488-conjugated goat anti-mouse (green channel) secondary antibodies. DAPI was used to stain the nuclei. White arrows denote invaded parasites (as detected by DAPI), and yellow arrowheads show the MIC2 staining dots near invaded Δ*rom1* Δ*rom4* Δ*rom5* parasites. (B) Quantification of fluorescent signals from extracellular versus intracellular parasites in panel A. ***, $P < 0.001$; NS, not significant. Two-way ANOVA with Bonferroni posttests. Representative data from two independent experiments with similar patterns. (C) Detection of MIC2 on the surface of triple knockout parasites during invasion. Freshly purified Δ*rom1* Δ*rom4* Δ*rom5* parasites were preinduced for microneme secretion and then allowed to invade HFF monolayers for 2 min. Samples were then fixed immediately and permeabilized for immunostaining. MIC2 was detected with MAb 6D10 followed by Alexa 488-conjugated goat anti-mouse IgG. The moving junction (MJ) was visualized by RON4 stained with rabbit anti-TgRON4 and Alexa 594-conjugated secondary antibody. Representative images with parasites at different stages of invasion are shown. White arrows indicate MJ. (D) Costaining of MIC2 dots with antibodies against the ectodomain ($MIC2_{ec}$) and cytoplasmic domain ($MIC2_t$) of MIC2. Triple knockout parasites were treated the same as in panel A and used in an invasion assay. Following fixation and permeabilization, cells were stained with MAb 6D10 (mouse anti-$MIC2_{ec}$) and WU1169 (rabbit anti-g10-MIC2t) or WU1170 (rabbit anti-g10 as negative control). Primary antibodies were detected as in panel A. (E) Staining of MIC2 dots before (− saponin) and after (+ saponin) permeabilization. The Δ*rom1* Δ*rom4* Δ*rom5* parasites were treated and used in an invasion assay as in panel A; after fixation, the samples were stained with Alexa 488-conjugated MAb 6D10 (green channel) to detect MIC2 that was outside host cells. Following 0.1% saponin permeabilization, the samples were stained with unconjugated MAb 6D10 (to detect total MIC2 that was in or outside host cells) and rabbit anti-SAG1 (to detect parasites), which were subsequently visualized by Alexa 594-conjugated goat anti-mouse and Alexa 350-conjugated goat anti-rabbit secondary antibodies, respectively. Bar, 5 μm.

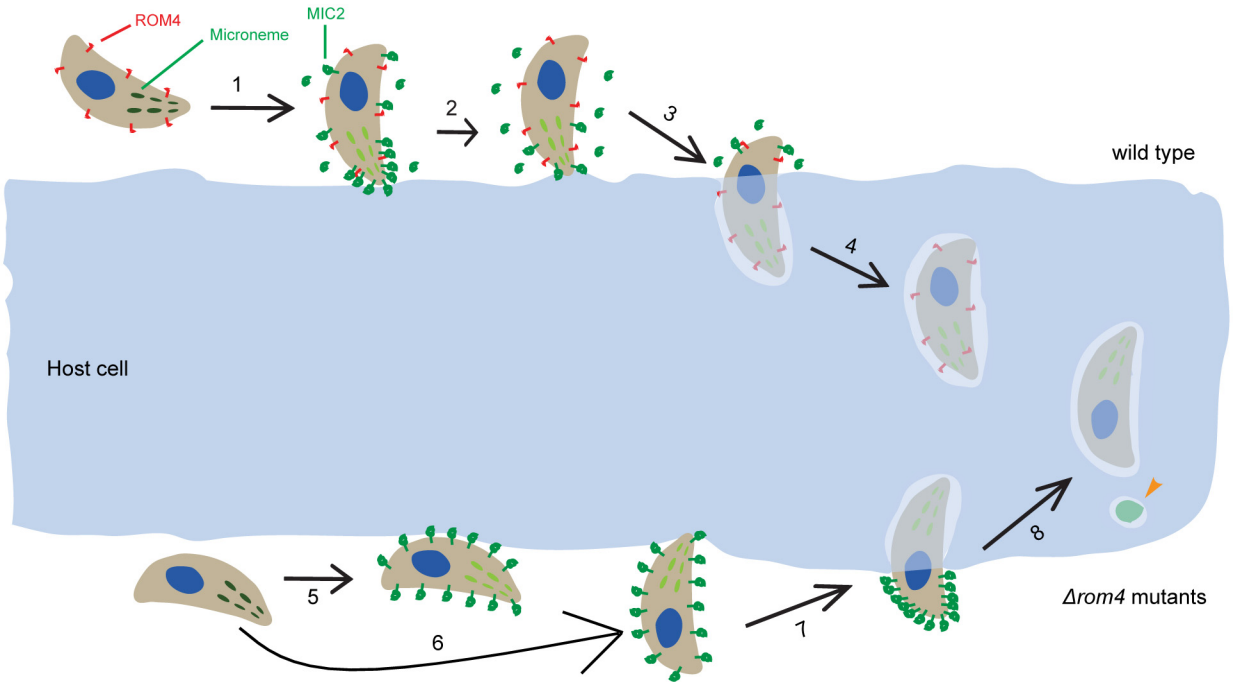

FIG 6 Model for MIC2 processing during invasion. Upon contact with host cells, parasites discharge their micronemal adhesins, including MIC2, to the surface from the apical end (step 1). MIC2 is then translocated to the posterior end by the motor complex (steps 1 to 3). In WT parasites (top), ROM4 is on the surface to cleave MIC2 to prevent aberrant host cell binding. Meanwhile, ROM4-mediated cleavage, along with the apical microneme secretion, allows MIC2 to form a temporal apical-to-posterior gradient that helps the parasite to reorientate and establish an MJ (step 1). Once MJ is formed, microneme secretion stops and surface MIC2 is shed by ROM4 (steps 2 and 3). The parasite starts to penetrate into the host cell (step 3), and no MIC2 is on the surface when it is fully internalized (step 4). *TgROM4*-deficient parasites (bottom) are not able to cleave surface MIC2. They lose the MIC2 gradient and often bind to host cells laterally (step 5); such nonproductive binding inhibits MJ formation and reduces invasion efficiency. However, if the mutant parasite does orientate correctly and form an MJ (step 6), it invades the host cell at normal speed (step 7). In addition, the unprocessed MIC2 that is accumulated on the surface is removed during active penetration and is capped behind the MJ (step 7). After its full entry, capped MIC2 is separated from the parasite (orange arrowhead) and accumulates within the host cell (step 8).

ally and in combination. All mutants were viable in tissue culture and had acute virulence in mice similar to that of wild-type parasites at a dose of 200 parasites/mouse. It is possible that there might be appreciable differences in virulence of Δ*rom* mutants in the type I background if a lower infection dose were used, or with a different strain background, such as less virulent type II strains. In addition, ROMs may play roles in other stages (such as bradyzoites) of the parasite's life cycle, where ROM4 is highly expressed. We were not able to test the role of ROM4 in bradyzoites due to the intrinsic defect in differentiation of the RH strain; however, such phenotypes could be explored using type II strains, which readily differentiate *in vitro* and *in vivo*. Nonetheless, our analyses conducted in tachyzoites of a type I strain indicated that TgROM4 is the primary protease required for efficient AMA1 and MIC2 shedding. It was somewhat surprising to find that ROM4 was important for micronemal adhesin processing, whereas ROM5 did not play a major role in shedding, despite previous predictions that it would be essential for this process (13). This prediction was based on the fact that ROM5 localizes to the posterior end of the parasite surface and that it has the most robust activity against diverse substrates in a heterologous COS7 cell system (13). However, our results do not support a major role for ROM5 in *T. gondii*, since its deletion did not have any obvious adhesin processing or invasion phenotype. In contrast, although ROM4 was critical for adhesin shedding in *T. gondii* parasites, when expressed in COS7 cells it did not show any protease activity (13). The basis for this discrepancy between activity in COS7 cells and that in the parasite is currently unknown, but possible explanations include that (i) factors that regulate the substrate specificity and protease activity of ROMs may be unique to *T. gondii* and (ii) membrane composition and thickness may be different in COS7 versus *T. gondii* cells, which in turn may affect substrate processing by ROMs.

Although MIC2 was not processed by Δ*rom4* mutants, this adhesin was stripped off the surface and capped from the posterior end as the parasite moved through the MJ (Fig. 6), indicating the existence of a ROM-independent mechanism for adhesin removal during host cell penetration. The molecular nature of this mechanism is not yet known; however, it does not involve alternative proteolytic processing, as the protein was still full length after removal from the parasite surface. Removal of surface MIC2 may occur as a result of sieving at the MJ, since such a role has been proposed before to exclude host membrane proteins from the parasitophorous vacuolar membrane (39). In contrast, AMA1 traversed the MJ and largely remained on the surface of invaded parasites, suggesting that removal of surface adhesins is not a universal process. The retention of AMA1 on intracellular parasites, while MIC2 was almost completely removed, is also consistent with the differences in processing of these two substrates by extracellular parasites. Although the basis for this difference in processing is not known, it suggests that the defect in MIC2 processing contributes more to the phenotype of the Δ*rom4* mutants than

does the defect in AMA1 processing. Consistent with this, *T. gondii* mutants of AMA1 that are refractory to rhomboid processing have only a modest effect on invasion and do not cause significant nonproductive adhesion as the Δ*rom4* mutants (28).

Proteolytic shedding of surface adhesins is a common feature in apicomplexan parasites: however, there are differences between species in the complexity and essentiality of this pathway. Unlike *T. gondii*, alternative adhesin processing seems to be common in *Plasmodium*. For example, thrombospondin-related anonymous protein (TRAP), a MIC2 homolog in *Plasmodium berghei*, is mainly cleaved by ROMs within the membrane but can also be cleaved by another protease outside the membrane, albeit with lower efficiency (40). Similarly, shedding of AMA1 in *P. falciparum* is mediated predominately by SUB2 at a juxtamembrane site, but it can also be processed by ROMs within the membrane (41). The existence of alternative processing pathways in *Plasmodium* spp. implies that adhesin shedding is more important in these parasites than in *T. gondii*. Consistent with this, a noncleavable TRAP mutant of *P. berghei* resulted in nonmotile and noninfectious sporozoites (40), and shedding-resistant mutants of EBA175 and AMA1 could not be stably introduced into the genome of *P. falciparum* (36, 41). Finally, unlike the situation in *T. gondii*, where none of the tachyzoite-stage ROMs was essential, four out of the eight *P. berghei* ROM genes were refractory to gene deletion in the asexual blood stage (42). Included in these putatively essential ROMs is *P. berghei* ROM4 (PbROM4), which is the orthologue of TgROM4, highlighting key differences in the essentiality of these pathways between these two parasites.

Our studies demonstrate that in *T. gondii*, ROM4 is the primary rhomboid protease required for efficient adhesin processing, and knockout mutants studied here behaved similarly to the previously described *ROM4* conditional knockdown mutant (26) and the noncleavable MIC2 mutants (38). All three mutants lead to accumulation of unprocessed adhesins on the surface, resulting in unproductive host cell attachment and reduced invasion. Collectively, these data are consistent with the following model for adhesin shedding and function of ROM4 during invasion (Fig. 6). Initially, MIC2 is secreted at the apical end of the parasite surface upon contact with host cells (5). Subsequently, surface MIC2 molecules are translocated to the posterior end by the actin-myosin motor complex (43). ROM4 is uniformly present on the plasma membrane (13), where it cleaves MIC2 and similar transmembrane adhesins to release their extracellular domains into the supernatant. The process of polarized micronemal secretion, in conjunction with the action of ROM4, establishes a temporal apical-to-posterior gradient of MIC2 (26, 44) (Fig. 6). This polarized adhesin gradient helps the parasite to orientate properly so that its apical end contacts the host cell to promote MJ formation, a process that initiates active host cell penetration. In the absence of ROM4, adhesins released from micronemes disperse to occupy the whole surface of the parasite and disrupt this gradient, leading to unproductive binding and impairing active invasion.

Our studies suggest a different role for rhomboids in *T. gondii* than that previously proposed. Although ROM4 is not essential for cell penetration, it functions to process surface adhesins in *T. gondii* in order to maintain a gradient that favors apical attachment and MJ formation. Removal of excess adhesins from the cell surface by ROMs facilitates efficient host cell invasion *in vitro* and may also aid immune evasion by clearing surface adhesins that might be targeted by neutralizing antibodies *in vivo*.

MATERIALS AND METHODS

Parasite strains and growth conditions. The RH Δ*ku80* Δ*hxgprt* strain (45) was used to generate all the genetically modified lines used in this study. All strains were maintained as tachyzoites by growth on monolayers of human foreskin fibroblasts (HFFs) in Dulbecco's modified Eagle's medium (DMEM; Life Technologies, Carlsbad, CA) supplemented with 10% fetal bovine serum (FBS) (Thermo Fisher Scientific, Waltham, MA) and 20 μg/ml gentamicin. Parasites used in experiments were freshly purified with 3-μm Nuclepore filters to remove host cell debris, as described previously (26).

Generating constructs to flox the *ROM* loci. Plasmids generated and used in this study are listed in Table S1 in the supplemental material. All *ROM* floxing constructs contain three fragments that were ligated together by LR reactions of corresponding entry vectors generated by BP cloning (Life Technologies, Carlsbad, CA). The fragments include the 5′ untranslated region (UTR) and 3′ UTR of each *ROM* gene surrounding a middle fragment containing loxP sites that flanked the *ROM* coding sequence and the selectable marker *HXGPRT* (Fig. 1A contains an illustration). The 5′ UTR and 3′ UTR of each *ROM* gene were amplified from RH genomic DNA (using primers listed in Table S2 in the supplemental material) and cloned into pDONR-P4P1r and pDONR-P2rP3, respectively. The middle fragment of each *ROM* gene was amplified (using primers listed in Table S2) from templates indicated in Table S1 and cloned into pDONR221 by BP cloning. The template vectors containing the middle fragments of *ROM* genes were generated as follows. For *ROM1*, the *HXGPRT* selection cassette obtained from pUNIV-KI by SpeI digestion was inserted into pS1HA9-ROM1 (25) at the SpeI site to give the plasmid pHA-ROM1/HXGPRT. For *ROM4*, the *HA-ROM4* coding sequence was amplified (primers listed in Table S2) from pS1HA9-ROM4 (26) and cloned into pUNIV-KI. For *ROM5*, exon 1 of *TgROM5* was amplified from RH genomic DNA (using primers listed in Table S2) and cloned into pUNIV-KI between the NcoI and EcoRI sites. Subsequently, the rest of the *ROM5* coding sequence was amplified (primers indicated in Table S2) from a previously published *HA-ROM5* construct (13) and cloned into pUNIV-KI-Exon 1 at the EcoRI site.

Generation of *ROM* knockout and complementing strains. To generate transgenic parasites with floxed *ROM* loci, the floxing plasmids were digested using restriction endonucleases (pDEST-loxP-HAR1 was digested with PciI to generate a 5.5-kb fragment, pDEST-loxP-HAR4 was digested with NdeI and PstI to generate a 6.7-kb fragment, and pDEST-loxP-R5Ty was digested with BglII and PciI to generate a 7.4-kb fragment) to expose both ends for homologous recombination. The digestion products were electroporated into RH Δ*ku80* Δ*hxgprt*, or indicated strains, as previously described (46). Parasites were subsequently selected with 25 μg/ml mycophenolic acid and 50 μg/ml xanthine (Sigma-Aldrich, St. Louis, MO), and single-cell clones were obtained by limiting dilution. Positive clones were identified by diagnostic PCR using primers listed in Table S2 in the supplemental material.

To knock out the *ROM* genes in the floxed strains, the Cre recombinase-expressing plasmid pmin-Cre-eGFP (31) was transiently introduced into the *ROM* floxed strains by electroporation and selected the loss of HXGPRT with 200 μg/ml 6-thioxanthine. *ROM* knockout clones were identified by PCR4 that confirmed the junction of loxP after *ROM* removal. The expression of ROMs in the floxed and deletion strains was further confirmed by Western blotting using antibodies raised from the N termini of ROM4 and ROM5, respectively (see below). The deletion of *ROM1* was confirmed by two additional PCRs (PCR5 and PCR6; primers listed in Table S2 in the supplemental material) to detect the endogenous *ROM1* gene.

To complement *ROM4* at the endogenous locus, the *ROM4* floxing construct digested with NdeI and PstI was transfected into Δ*rom4* and Δ*rom1* Δ*rom4* Δ*rom5* strains and selected with 25 μg/ml mycophenolic acid and 50 μg/ml xanthine. After limiting dilution, positive clones were identified by diagnostic PCR described as above, and ROM4 expression was confirmed by Western blotting.

Production of antibodies against TgROM4 and TgROM5. Recombinant proteins corresponding to the N termini of TgROM4 (R4n, containing residues V25 to G240 of TgROM4) and TgROM5 (R5n, containing residues M1 to R319 of TgROM5) were expressed and purified from BL21(DE3)/pLysS containing pET28a-R4n and pET16b-R5n (plasmids listed in Table S1 in the supplemental material), respectively. A New Zealand White rabbit (Covance, Princeton, NJ) (R4n) or CD-1 mice (Charles River Laboratories, Wilmington, MA) (R5n) were injected with purified antigens and boosted two more times after initial injection. Subsequently, the animals were sacrificed and sera were collected for analysis.

Plaque assay. Purified parasites were used to infect fresh host cell monolayers seeded in 6-well plates and grown for 7 days without movement. Cells were then fixed with 70% ethanol and stained with 0.1% crystal violet. Plaques were scanned using an Epson scanner and analyzed as previously reported (47). Experiments were repeated three times independently, and each strain was assayed in triplicate within each experiment.

Virulence assay. Freshly egressed parasites were intraperitoneally injected into CD-1 female mice (200 parasites/mouse and 5 mice/strain). The survival of mice was monitored, and data were analyzed as previously described (48).

Invasion assay. A previously established two-color staining protocol (26) that distinguished extracellular and intracellular parasites was used to determine the host cell invasion efficiencies of the *ROM* mutants, with the following modifications: the invasion assay was done using host cells seeded in 96-well plates, and after staining, the plates were imaged on the Cytation 3 cell imaging multimode reader (BioTek, Winooski, VT). Data were analyzed with Gen5 software (BioTek, Winooski, VT). Experiments were repeated three times independently (each with triplicates).

Time-lapse microscopy assay of parasite motility and invasion. To visualize parasite motility, freshly egressed tachyzoites were purified and resuspended in intracellular buffer (5 mM NaCl, 142 mM KCl, 2 mM EGTA, 1 mM $MgCl_2$, 5.6 mM glucose, 25 mM HEPES-KOH, pH 7.2) (49) before analysis. Motility was induced by adding parasites to BSA-coated glass-bottom culture dishes (MatTek, Ashland, MA) that contained Ringer's buffer (155 mM NaCl, 3 mM KCl, 2 mM $CaCl_2$, 1 mM $MgCl_2$, 3 mM NaH_2PO_4, 10 mM HEPES, 10 mM glucose, pH 7.2), as previously described (26). Parasites were then kept at 37°C with Tempcontrol 37-2 (Carl Zeiss, Inc., Thornwood, NY) and imaged on the Zeiss Axio Observer Z1 time-lapse imaging system (Carl Zeiss, Inc., Thornwood, NY) under ×40 magnification for 3 min at 1 frame/s. Motility patterns were analyzed as previously described (26).

To measure the speed of invasion, freshly purified parasites were resuspended in invasion medium (DMEM, 20 mM HEPES, 3% FBS, pH 7.4), used to infect HFF host cells seeded on glass-bottom culture dishes, and imaged as described above. The time of each invasion event (from apical binding to complete internalization) was used to estimate invasion speed. Each strain was analyzed in two independent experiments, and each experiment contained 20 to 30 invasion events taken from 4 to 6 movies.

Intracellular replication assay. Replication of indicated strains within host cells was determined as previously described (47). After SAG1 staining, the number of vacuoles containing the indicated number of parasites (i.e., 1, 2, 4, or 8 cells) was counted from ≥100 vacuoles from three separate coverslips per experiment. Two independent experiments were conducted, and combined results were graphed.

Microneme secretion assay. Microneme secretion was monitored based on the release of adhesins into culture supernatants as previously described (26). In brief, purified tachyzoites (10^8 in 100 μl) were induced with 3% FBS plus 1% ethanol in invasion medium at 37°C for 15 min. Subsequently, supernatants were separated from pelleted cells by centrifugation (400 × *g* for 10 min), and the proteins of interest in each fraction were analyzed by Western blotting. Samples from each strain (25% of the supernatant fractions and 10% of the pellet fractions) were resolved on 10% SDS-PAGE gels and analyzed by Western blotting. MIC2 and AMA1 were detected by monoclonal antibodies (MAbs) 6D10 (9) and B3.90 (50), respectively. TgALD was detected by rabbit anti-TgALD (51), and MIC5 was detected with rabbit anti-TgMIC5 (52). Primary antibodies were detected with Li-Cor secondary antibodies (Life Technologies, Carlsbad, CA), and blots were developed on the Li-Cor Odyssey infrared imaging system (Li-Cor Biosciences, Lincoln, NE).

Moving junction formation. Freshly isolated parasites were allowed to invade HFF monolayers in invasion medium at 37°C for 5 min. Samples were then immediately fixed with 4% paraformaldehyde, stained, and examined by epifluorescence microscopy as previously described (26). Each strain was tested in three independent experiments, each with triplicates.

Quantification of surface adhesin levels on parasites. Freshly egressed parasites of the WT and Δ*rom1* Δ*rom4* Δ*rom5* strains were treated with 3% FBS plus 1% ethanol to induce their microneme secretion for 15 min in invasion medium. Subsequently, they were allowed to invade HFF monolayers for 5 min, fixed with 4% paraformaldehyde, and subjected to immunostaining. Samples were first stained with rabbit anti-SAG1 followed by Alexa 594-conjugated goat anti-rabbit secondary antibody. Following 0.1% saponin permeabilization, samples were stained with MAb 6D10 (for MIC2), MAb B3.90 (for AMA1), or MAb DG52 (for SAG1) and visualized by Alexa 488-conjugated goat anti-mouse secondary antibody. Parasite and host nuclei were stained by 4′,6-diamidino-2-phenylindole (DAPI). Images were acquired using a Zeiss Axioskop 2 MOT Plus microscope equipped with a 63× numerical-aperture (NA)-1.6 oil immersion lens and an AxioCam MRm Monochrome camera (Carl Zeiss, Inc., Thornwood, NY). Fluorescent signals were quantified by the Volocity software (PerkinElmer, Waltham, MA). Two independent experiments (each with triplicates) were conducted.

Distribution of surface MIC2 during invasion. Freshly purified parasites were induced for microneme secretion as described above and subsequently allowed to invade HFF monolayers for 2 min at 37°C. Parasites were immediately fixed with 4% paraformaldehyde and permeabilized with 0.1% saponin. MIC2 was detected by MAb 6D10 followed by Alexa 488-conjugated goat anti-mouse secondary antibody, and RON4 was visualized by rabbit anti-TgRON4 followed by Alexa 594-conjugated goat anti-rabbit secondary antibody. Images were acquired as described above.

Flow cytometry and fluorescence microscopy of surface MIC2. Purified parasites were induced for microneme secretion as described above and subsequently fixed with 4% paraformaldehyde for immunostaining. MIC2 was stained with MAb 6D10. SAG1 was detected by MAb DG52, and ChromPure mouse IgG (Jackson ImmunoResearch Laboratories, Inc., West Grove, PA) was used as a negative control. Primary antibodies were stained with Alexa 488-conjugated goat anti-mouse secondary antibody. Samples were analyzed by flow cytometry using FACSCanto (Becton, Dickinson, Franklin Lakes, NJ) as previously described (26).

To visualize MIC2 by fluorescence microscopy, parasites were prepared in the same way as that described above but costained with rabbit anti-SAG1 and MAb 6D10 and examined by epifluorescence microscopy as described above.

RT-PCR. Total RNA from parasites was extracted with the RNeasy kit (Qiagen Inc., Valencia, CA), and 400 ng RNA was subjected to reverse transcription using SuperScript III reverse transcriptase according to the manufacturer's instructions (Life Technologies, Carlsbad, CA). Subsequently, quantitative PCR was performed using the SYBR green master mix (Life Technologies, Carlsbad, CA) containing corresponding primer pairs (see Table S1 in the supplemental material) as previously described (26). Total RNA isolated from unsporulated oocysts (provided by John Boothroyd) was used as a positive control for *TgROM2* or *TgROM3* expression. Three independent experiments were performed, and combined results were reported.

Statistics. Statistical comparisons were conducted in Prism (GraphPad Software, Inc., La Jolla, CA) using one-way analysis of variance (ANOVA) and Bonferroni's multiple comparison posttests. For comparing two groups that contain multiple data sets, two-way ANOVA with

Bonferroni multiple comparison posttests was used. Significant differences across all repeated experiments are indicated.

SUPPLEMENTAL MATERIAL

Supplemental material for this article may be found at http://mbio.asm.org/lookup/suppl/doi:10.1128/mBio.01795-14/-/DCSupplemental.

Figure S1, PDF file, 0.3 MB.
Figure S2, PDF file, 0.5 MB.
Table S1, PDF file, 0.03 MB.
Table S2, PDF file, 0.1 MB.

ACKNOWLEDGMENTS

We are grateful to Gary Ward, Vern Carruthers, and John Boothroyd for providing antibodies; Ke Hu for the Cre-expressing plasmid; members of the Sibley lab and Dominique Soldati-Favre for helpful discussions; and Jennifer Barks and Qiuling Wang for technical assistance.

The work was supported by a grant from the NIH (AI034036).

REFERENCES

1. **Elmore SA, Jones JL, Conrad PA, Patton S, Lindsay DS, Dubey JP.** 2010. *Toxoplasma gondii*: epidemiology, feline clinical aspects, and prevention. Trends Parasitol. **26:**190–196. http://dx.doi.org/10.1016/j.pt.2010.01.009.
2. **Shen B, Sibley LD.** 2012. The moving junction, a key portal to host cell invasion by apicomplexan parasites. Curr. Opin. Microbiol. **15:**449–455. http://dx.doi.org/10.1016/j.mib.2012.02.007.
3. **Sharma P, Chitnis CE.** 2013. Key molecular events during host cell invasion by apicomplexan pathogens. Curr. Opin. Microbiol. **16:**432–437. http://dx.doi.org/10.1016/j.mib.2013.07.004.
4. **Soldati D, Dubremetz JF, Lebrun M.** 2001. Microneme proteins: structural and functional requirements to promote adhesion and invasion by the apicomplexan parasite *Toxoplasma gondii*. Int. J. Parasitol. **31:**1293–1302. http://dx.doi.org/10.1016/S0020-7519(01)00257-0.
5. **Carruthers VB, Sibley LD.** 1997. Sequential protein secretion from three distinct organelles of *Toxoplasma gondii* accompanies invasion of human fibroblasts. Eur. J. Cell Biol. **73:**114–123.
6. **Lebrun M, Michelin A, El Hajj H, Poncet J, Bradley PJ, Vial H, Dubremetz JF.** 2005. The rhoptry neck protein RON4 re-localizes at the moving junction during *Toxoplasma gondii* invasion. Cell. Microbiol. **7:**1823–1833. http://dx.doi.org/10.1111/j.1462-5822.2005.00646.x.
7. **Alexander DL, Mital J, Ward GE, Bradley P, Boothroyd JC.** 2005. Identification of the moving junction complex of *Toxoplasma gondii*: a collaboration between distinct secretory organelles. PLoS Pathog. **1:**e17. http://dx.doi.org/10.1371/journal.ppat.0010017.
8. **Carruthers VB.** 2006. Proteolysis and toxoplasma invasion. Int. J. Parasitol. **36:**595–600. http://dx.doi.org/10.1016/j.ijpara.2006.02.008.
9. **Carruthers VB, Sherman GD, Sibley LD.** 2000. The toxoplasma adhesive protein MIC2 is proteolytically processed at multiple sites by two parasite-derived proteases. J. Biol. Chem. **275:**14346–14353. http://dx.doi.org/10.1074/jbc.275.19.14346.
10. **Zhou XW, Blackman MJ, Howell SA, Carruthers VB.** 2004. Proteomic analysis of cleavage events reveals a dynamic two-step mechanism for proteolysis of a key parasite adhesive complex. Mol. Cell. Proteomics **3:**565–576. http://dx.doi.org/10.1074/mcp.M300123-MCP200.
11. **Lagal V, Binder EM, Huynh MH, Kafsack BF, Harris PK, Diez R, Chen D, Cole RN, Carruthers VB, Kim K.** 2010. *Toxoplasma gondii* protease TgSUB1 is required for cell surface processing of micronemal adhesive complexes and efficient adhesion of tachyzoites. Cell. Microbiol. **12:**1792–1808. http://dx.doi.org/10.1111/j.1462-5822.2010.01509.x.
12. **Opitz C, Di Cristina M, Reiss M, Ruppert T, Crisanti A, Soldati D.** 2002. Intramembrane cleavage of microneme proteins at the surface of the apicomplexan parasite *Toxoplasma gondii*. EMBO J. **21:**1577–1585. http://dx.doi.org/10.1093/emboj/21.7.1577.
13. **Brossier F, Jewett TJ, Sibley LD, Urban S.** 2005. A spatially localized rhomboid protease cleaves cell surface adhesins essential for invasion by Toxoplasma. Proc. Natl. Acad. Sci. U. S. A. **102:**4146–4151. http://dx.doi.org/10.1073/pnas.0407918102.
14. **Dowse TJ, Pascall JC, Brown KD, Soldati D.** 2005. Apicomplexan rhomboids have a potential role in microneme protein cleavage during host cell invasion. Int. J. Parasitol. **35:**747–756. http://dx.doi.org/10.1016/j.ijpara.2005.04.001.
15. **Freeman M.** 2008. Rhomboid proteases and their biological functions. Annu. Rev. Genet. **42:**191–210. http://dx.doi.org/10.1146/annurev.genet.42.110807.091628.
16. **Urban S.** 2009. Making the cut: central roles of intramembrane proteolysis in pathogenic microorganisms. Nat. Rev. Microbiol. **7:**411–423.
17. **Urban S, Dickey SW.** 2011. The rhomboid protease family: a decade of progress on function and mechanism. Genome Biol. **12:**231. http://dx.doi.org/10.1186/gb-2011-12-10-231.
18. **Urban S, Freeman M.** 2003. Substrate specificity of rhomboid intramembrane proteases is governed by helix-breaking residues in the substrate transmembrane domain. Mol. Cell **11:**1425–1434. http://dx.doi.org/10.1016/S1097-2765(03)00181-3.
19. **Urban S, Schlieper D, Freeman M.** 2002. Conservation of intramembrane proteolytic activity and substrate specificity in prokaryotic and eukaryotic rhomboids. Curr. Biol. **12:**1507–1512. http://dx.doi.org/10.1016/S0960-9822(02)01092-8.
20. **Baker RP, Wijetilaka R, Urban S.** 2006. Two Plasmodium rhomboid proteases preferentially cleave different adhesins implicated in all invasive stages of malaria. PLoS Pathog. **2:**e113. http://dx.doi.org/10.1371/journal.ppat.0020113.
21. **Baxt LA, Baker RP, Singh U, Urban S.** 2008. An Entamoeba histolytica rhomboid protease with atypical specificity cleaves a surface lectin involved in phagocytosis and immune evasion. Genes Dev. **22:**1636–1646. http://dx.doi.org/10.1101/gad.1667708.
22. **Dickey SW, Baker RP, Cho S, Urban S.** 2013. Proteolysis inside the membrane is a rate-governed reaction not driven by substrate affinity. Cell **155:**1270–1281. http://dx.doi.org/10.1016/j.cell.2013.10.053.
23. **Dowse TJ, Soldati D.** 2005. Rhomboid-like proteins in Apicomplexa: phylogeny and nomenclature. Trends Parasitol. **21:**254–258. http://dx.doi.org/10.1016/j.pt.2005.04.009.
24. **Sibley LD.** 2013. The roles of intramembrane proteases in protozoan parasites. Biochim. Biophys. Acta **1828:**2908–2915. http://dx.doi.org/10.1016/j.bbamem.2013.04.017.
25. **Brossier F, Starnes GL, Beatty WL, Sibley LD.** 2008. Microneme rhomboid protease TgROM1 is required for efficient intracellular growth of *Toxoplasma gondii*. Eukaryot. Cell **7:**664–674. http://dx.doi.org/10.1128/EC.00331-07.
26. **Buguliskis JS, Brossier F, Shuman J, Sibley LD.** 2010. Rhomboid 4 (ROM4) affects the processing of surface adhesins and facilitates host cell invasion by *Toxoplasma gondii*. PLoS Pathog. **6:**e1000858. http://dx.doi.org/10.1371/journal.ppat.1000858.
27. **Santos JM, Ferguson DJ, Blackman MJ, Soldati-Favre D.** 2011. Intramembrane cleavage of AMA1 triggers Toxoplasma to switch from an invasive to a replicative mode. Science **331:**473–477. http://dx.doi.org/10.1126/science.1199284.
28. **Parussini F, Tang Q, Moin SM, Mital J, Urban S, Ward GE.** 2012. Intramembrane proteolysis of Toxoplasma apical membrane antigen 1 facilitates host-cell invasion but is dispensable for replication. Proc. Natl. Acad. Sci. U. S. A. **109:**7463–7468. http://dx.doi.org/10.1073/pnas.1114661109.
29. **Bargieri DY, Andenmatten N, Lagal V, Thiberge S, Whitelaw JA, Tardieux I, Meissner M, Menard R.** 2013. Apical membrane antigen 1 mediates apicomplexan parasite attachment but is dispensable for host cell invasion. Nat. Commun. **4:**2552. http://dx.doi.org/10.1038/ncomms3552.
30. **Brecht S, Erdhart H, Soete M, Soldati D.** 1999. Genome engineering of *Toxoplasma gondii* using the site-specific recombinase Cre. Gene **234:**239–247. http://dx.doi.org/10.1016/S0378-1119(99)00202-4.
31. **Heaslip AT, Nishi M, Stein B, Hu K.** 2011. The motility of a human parasite, *Toxoplasma gondii*, is regulated by a novel lysine methyltransferase. PLoS Pathog. **7:**e1002201. http://dx.doi.org/10.1371/journal.ppat.1002201.
32. **Lamarque MH, Roques M, Kong-Hap M, Tonkin ML, Rugarabamu G, Marq JB, Penarete-Vargas DM, Boulanger MJ, Soldati-Favre D, Lebrun M.** 2014. Plasticity and redundancy among AMA-RON pairs ensure host cell entry of Toxoplasma parasites. Nat. Commun **5:**4098. http://dx.doi.org/10.1038/ncomms5098.
33. **Huynh MH, Carruthers VB.** 2006. Toxoplasma MIC2 is a major determinant of invasion and virulence. PLoS Pathog. **2:**e84. http://dx.doi.org/10.1371/journal.ppat.0020084.
34. **Mital J, Meissner M, Soldati D, Ward GE.** 2005. Conditional expression of *Toxoplasma gondii* apical membrane antigen-1 (TgAMA1) demon-

strates that TgAMA1 plays a critical role in host cell invasion. Mol. Biol. Cell **16:**4341–4349. http://dx.doi.org/10.1091/mbc.E05-04-0281.

35. **Brydges SD, Sherman GD, Nockemann S, Loyens A, Daubener W, Dubremetz JF, Carruthers VB.** 2000. Molecular characterization of TgMIC5, a proteolytically processed antigen secreted from the micronemes of *Toxoplasma gondii*. Mol. Biochem. Parasitol. **111:**51–66. http://dx.doi.org/10.1016/S0166-6851(00)00296-6.
36. **O'Donnell RA, Hackett F, Howell SA, Treeck M, Struck N, Krnajski Z, Withers-Martinez C, Gilberger TW, Blackman MJ.** 2006. Intramembrane proteolysis mediates shedding of a key adhesin during erythrocyte invasion by the malaria parasite. J. Cell Biol. **174:**1023–1033. http://dx.doi.org/10.1083/jcb.200604136.
37. **Howell SA, Hackett F, Jongco AM, Withers-Martinez C, Kim K, Carruthers VB, Blackman MJ.** 2005. Distinct mechanisms govern proteolytic shedding of a key invasion protein in apicomplexan pathogens. Mol. Microbiol. **57:**1342–1356. http://dx.doi.org/10.1111/j.1365-2958.2005.04772.x.
38. **Brossier F, Jewett TJ, Lovett JL, Sibley LD.** 2003. C-terminal processing of the toxoplasma protein MIC2 is essential for invasion into host cells. J. Biol. Chem. **278:**6229–6234. http://dx.doi.org/10.1074/jbc.M209837200.
39. **Mordue DG, Desai N, Dustin M, Sibley LD.** 1999. Invasion by *Toxoplasma gondii* establishes a moving junction that selectively excludes host cell plasma membrane proteins on the basis of their membrane anchoring. J. Exp. Med. **190:**1783–1792. http://dx.doi.org/10.1084/jem.190.12.1783.
40. **Ejigiri I, Ragheb DR, Pino P, Coppi A, Bennett BL, Soldati-Favre D, Sinnis P.** 2012. Shedding of TRAP by a rhomboid protease from the malaria sporozoite surface is essential for gliding motility and sporozoite infectivity. PLoS Pathog. **8:**e1002725. http://dx.doi.org/10.1371/journal.ppat.1002725.
41. **Olivieri A, Collins CR, Hackett F, Withers-Martinez C, Marshall J, Flynn HR, Skehel JM, Blackman MJ.** 2011. Juxtamembrane shedding of Plasmodium falciparum AMA1 is sequence independent and essential, and helps evade invasion-inhibitory antibodies. PLoS Pathog. **7:**e1002448. http://dx.doi.org/10.1371/journal.ppat.1002448.
42. **Lin JW, Meireles P, Prudencio M, Engelmann S, Annoura T, Sajid M, Chevalley-Maurel S, Ramesar J, Nahar C, Avramut CM, Koster AJ, Matuschewski K, Waters AP, Janse CJ, Mair GR, Khan SM.** 2013. Loss-of-function analyses defines vital and redundant functions of the Plasmodium rhomboid protease family. Mol. Microbiol. **88:**318–338. http://dx.doi.org/10.1111/mmi.12187.
43. **Carruthers VB, Sibley LD.** 1999. Mobilization of intracellular calcium stimulates microneme discharge in *Toxoplasma gondii*. Mol. Microbiol. **31:**421–428. http://dx.doi.org/10.1046/j.1365-2958.1999.01174.x.
44. **Carruthers VB, Giddings OK, Sibley LD.** 1999. Secretion of micronemal proteins is associated with toxoplasma invasion of host cells. Cell. Microbiol. **1:**225–235. http://dx.doi.org/10.1046/j.1462-5822.1999.00023.x.
45. **Huynh MH, Carruthers VB.** 2009. Tagging of endogenous genes in a *Toxoplasma gondii* strain lacking Ku80. Eukaryot. Cell **8:**530–539. http://dx.doi.org/10.1128/EC.00358-08.
46. **Soldati D, Boothroyd JC.** 1993. Transient transfection and expression in the obligate intracellular parasite *Toxoplasma gondii*. Science **260:**349–352. http://dx.doi.org/10.1126/science.8469986.
47. **Shen B, Sibley LD.** 2014. Toxoplasma aldolase is required for metabolism but dispensable for host-cell invasion. Proc. Natl. Acad. Sci. U. S. A. **111:**3567–3572. http://dx.doi.org/10.1073/pnas.1315156111.
48. **Etheridge RD, Alaganan A, Tang K, Lou HJ, Turk BE, Sibley LD.** 2014. The Toxoplasma pseudokinase ROP5 forms complexes with ROP18 and ROP17 kinases that synergize to control acute virulence in mice. Cell Host Microbe **15:**537–550. http://dx.doi.org/10.1016/j.chom.2014.04.002.
49. **Moudy R, Manning TJ, Beckers CJ.** 2001. The loss of cytoplasmic potassium upon host cell breakdown triggers egress of *Toxoplasma gondii*. J. Biol. Chem. **276:**41492–41501. http://dx.doi.org/10.1074/jbc.M106154200.
50. **Donahue CG, Carruthers VB, Gilk SD, Ward GE.** 2000. The toxoplasma homolog of Plasmodium apical membrane antigen-1 (AMA-1) is a microneme protein secreted in response to elevated intracellular calcium levels. Mol. Biochem. Parasitol. **111:**15–30. http://dx.doi.org/10.1016/S0166-6851(00)00289-9.
51. **Starnes GL, Jewett TJ, Carruthers VB, Sibley LD.** 2006. Two separate, conserved acidic amino acid domains within the *Toxoplasma gondii* MIC2 cytoplasmic tail are required for parasite survival. J. Biol. Chem. **281:**30745–30754. http://dx.doi.org/10.1074/jbc.M606523200.
52. **Brydges SD, Zhou XW, Huynh MH, Harper JM, Mital J, Adjogble KD, Daubener W, Ward GE, Carruthers VB.** 2006. Targeted deletion of MIC5 enhances trimming proteolysis of Toxoplasma invasion proteins. Eukaryot. Cell **5:**2174–2183. http://dx.doi.org/10.1128/EC.00163-06.